View metadata, citation and similar papers at core.ac.uk

brought to you by CORE

provided by Digital.CSIC

Strong coupling of single emitters interacting with phononic infrared antennae

This content has been downloaded from IOPscience. Please scroll down to see the full text.

2014 New J. Phys. 16 013052

(http://iopscience.iop.org/1367-2630/16/1/013052)

View the table of contents for this issue, or go to the journal homepage for more

Download details:

IP Address: 161.111.180.191
This content was downloaded on 01/10/2014 at 08:19

Please note that terms and conditions apply.

New Journal of Physics
The open access journal at the forefront of physics
Deutsche Physikalische Gesellschaft DPG | IOP Institute of Physics

Strong coupling of single emitters interacting with phononic infrared antennae

Ruben Esteban[1,2,3], **Javier Aizpurua**[2] **and Garnett W Bryant**[1]

[1] Quantum Measurement Division and Joint Quantum Institute, National Institute of Standards and Technology and University of Maryland, Gaithersburg, MD 20899, USA
[2] Materials Physics Center CSIC-UPV/EHU and Donostia International Physics Center DIPC, Paseo Manuel de Lardizabal 5, E-20018 Donostia-San Sebastián, Spain
E-mail: ruben_esteban@ehu.es

Received 21 October 2013, revised 25 December 2013
Accepted for publication 7 January 2014
Published 30 January 2014

New Journal of Physics **16** (2014) 013052

doi:10.1088/1367-2630/16/1/013052

Abstract

A single emitter can couple with electromagnetic modes of dielectric cavities or metallic particles. In a similar manner, it can couple with a phononic mode supported by a nearby infrared antenna. We consider an emitter with a sufficiently large dipole moment coupled to a SiC bowtie structure supporting strongly localized phononic modes. We show that vacuum Rabi oscillations and large spectral anticrossing are possible, indicating that the emitter–phononic system is in the strong coupling regime. Pure dephasing degrades the response remarkably little. As expected for a quantum but not for a classical formalism, the frequency of the vacuum Rabi oscillations depends on the initial state. We also discuss the possibility of exciting hybrid modes with contributions from the emitter and from more than one of the phononic modes supported by the antenna. Phononic structures appear attractive to study such complex hybridization, as they can support several strongly confined modes with quality factors larger than one hundred in a relatively small spectral window.

The interaction between a single quantum emitter, such as a quantum dot or a nitrogen vacancy in diamond [1], and an electromagnetic mode can lead to a regime of strong coupling, where energy is transferred coherently between the mode and the emitter in this hybrid system.

[3] Author to whom any correspondence should be addressed.

Content from this work may be used under the terms of the Creative Commons Attribution 3.0 licence. Any further distribution of this work must maintain attribution to the author(s) and the title of the work, journal citation and DOI.

© 2014 IOP Publishing Ltd and Deutsche Physikalische Gesellschaft

To achieve strong coupling, it is beneficial for the electromagnetic mode to exhibit a large quality factor Q, and thus large lifetime, while being spatially confined to the smallest possible volume V. Much work exploits very high Q electromagnetic modes supported by dielectric resonators [2–6]. Due to the diffraction limit, however, the minimum modal volume in these systems for wavelength λ and optical constant of the dielectric n is $V \approx (\lambda/(2n))^3$, which for a given Q limits the achievable coupling strength $g \propto \sqrt{Q/V}$ between the emitter and the mode. Reaching the strong coupling regime in these dielectric systems also typically depends upon a very low pure dephasing rate γ_d of the emitter, a requirement less stringent for stronger g.

A different possibility is to exploit plasmonic resonances, which have low quality factors but are not constrained by the diffraction limit and can support modes with low modal volume, making large coupling strengths g possible. The large $|g|$ and broad resonances also reduce the demands on the pure dephasing and the tuning of the system. Metallic structures [7–18] are typically considered, but strong coupling with graphene plasmons also seems possible [19, 20].

Here, we show that strong coupling can also be achieved, in a similar manner as for plasmons, by using strongly confined phononic resonances, i.e. localized surface phonon–polaritons in polar materials. The coupling between the incoming photons and the phonons of certain materials leads to the excitation of these phonon–polaritons [21]. In particular, discrete SiC structures support localized surface phonon–polariton resonances [22, 23] at mid-infrared wavelengths near 11 μm. The relatively low absorption coefficient in SiC makes it possible to reach quality factors of $Q > 100$ [24], much lower than those in high Q dielectric cavities but larger than for typical plasmonic resonances in metallic structures, and comparable to expectations for graphene structures [19].

Low absorption losses can also have an indirect but significant impact on the coupling strength g via the modal volume V. The fields can be strongly localized in plasmonic or phononic modes because the material excitations are associated with evanescent fields that can decay very fast spatially. The minimum possible volume of the electromagnetic mode is thus not constrained by the diffraction limit and is extremely low [24–27]. However, field confinement is in practice often increased by using small particles, sharp edges or very narrow inter-particle gaps, which tend to result in a low radiative yield η, the probability that the decay of the excited system results in an emitted photon. Thus, when a large η is desired, low absorption losses relax the constraints on the geometry and are conducive to lower modal volumes and larger g.

Figure 1(a) sketches the geometry considered in our work, operating at excitation wavelengths $\gtrsim$10 μm. A single infrared emitter is situated in the middle of the gap of a SiC bowtie infrared antenna [28–30] formed by two cones capped, at the gap, by 10 nm spherical tips. The system is rotational symmetric with respect to the axis z and is situated in vacuum. Each cone is 1 μm long and the gap is 10 nm. All the dimensions, in particular in the gap region, are considerably smaller than the emission wavelength. To be near the phononic resonances, the emitter should be in the mid-infrared, which can be a challenge to achieve. We model the emitter as a two-level system oriented along the antenna axis z, with dipole moment d_z for the transition between the ground $|0\rangle$ and the excited $|1\rangle$ states.

We use the boundary element method (BEM) [31, 32] to obtain the classical electromagnetic response of the antenna itself, without the two-level emitter. An oscillator model [33–35] describes the SiC permittivity as a function of angular excitation frequency ω as $\varepsilon_{SiC} = \varepsilon_0\varepsilon_\infty[1 + (\omega_l^2 - \omega_t^2)/(\omega_t^2 - \omega^2 - i\omega\Gamma)]$. ε_0 is the vacuum permitivity, $\varepsilon_\infty = 6.7$ gives the asymptotic value of the relative permittivity at large energies, $\Gamma = 4.76\,\mathrm{cm}^{-1}$ determines the losses and $\omega_l = 969\,\mathrm{cm}^{-1}$ and $\omega_t = 793\,\mathrm{cm}^{-1}$ are the phonon angular frequencies associated

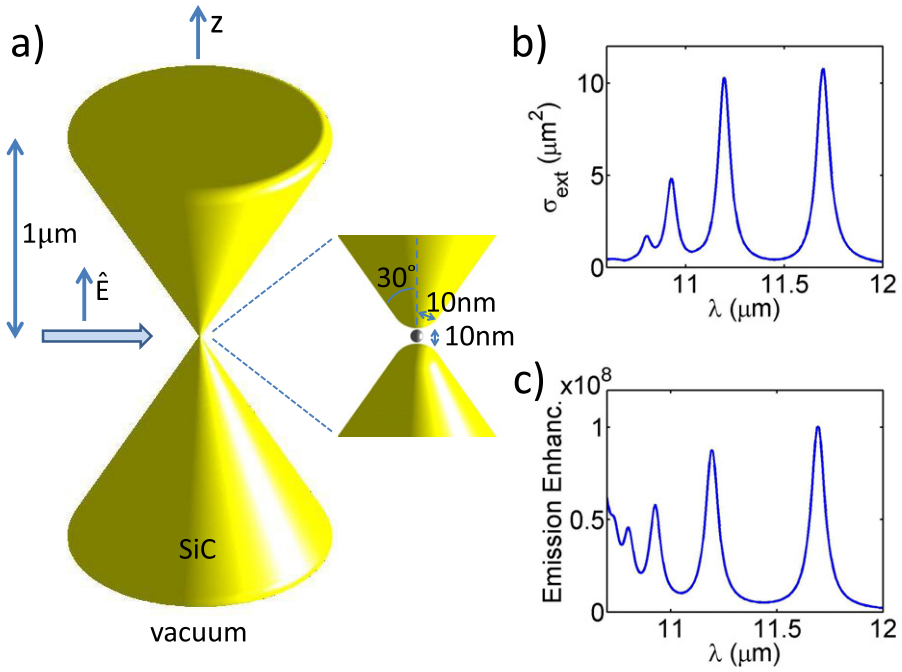

Figure 1. Diagram of the structure used and its classical response. (a) The SiC bowtie antennae are rotationally symmetric, placed in vacuum and formed by two 1 μm long cones with 10 nm radius spherical tips near the gap and with flat surfaces at the outside ends. The angle between the bowtie axis z and one generatrix line is 30°, and the flat ends are rounded using a 50 nm radius. For a quantum treatment of the system, a two-level emitter made of material with dielectric constant ε_e and dipole moment d_z is placed at the middle of the gap and polarized along z. We typically consider plane-wave excitation with electric field also polarized along z. The gap area is better observed in the zoom to the right of the full structure. (b) Extinction spectrum of the antenna, without emitter, under plane-wave illumination. (c) Enhancement of the energy dissipation rate of a classical dipole placed at the same position and with same z orientation as the quantum-mechanical two-level emitter in (a). The enhancement is normalized to the dissipation rate of the dipole in vacuum that would be obtained if no bowtie antenna were present.

with the longitudinal and transverse modes in the material respectively. ω_l and ω_t define the spectral region where the localized phononic resonances occur. We do not consider anisotropy or other, weaker, phononic contributions to ε_{SiC} that can be present in SiC polytypes [36–39]. Figure 1(b) shows the extinction cross-section of the SiC antenna under plane-wave illumination polarized along z, and figure 1(c) the enhancement of the rate of energy dissipation when the illumination source is a classical dipole situated at midgap and oriented like the emitter. This enhancement is given as the ratio of the dipole dissipation with and without antenna. It corresponds to the Purcell factor, defined as the decay rate increase that the emitter in figure 1(a) experiences due to the presence of the antenna, assuming there is no pure dephasing or intrinsic losses [40, 41], and the emitter is in the weak coupling regime [42].

Both spectra exhibit clear and relatively narrow resonances, corresponding to phononic electromagnetic modes at wavelengths λ_{ph}. The quality factor of, for example, the lowest energy peak in figure 1(b) at wavelength $\lambda_{ph} = 11.695\,\mu$m is $Q \approx 150$. The obtained Purcell factor

$F_p \approx 10^8$ is very large [24] even when compared to the already large values typically discussed for plasmonics systems [43, 44]. For this same resonance the scattering contribution is about 17% of the total extinction ($\approx$1.9 versus $\approx$11 μm^2), while about 16% of the energy dissipated by the dipole is radiated to the far field. Losses are thus significant in the hybrid system considered, but a non-negligible amount of photons should nonetheless be emitted and detectable by far-field detectors.

To model the quantum interaction between the emitter and one of the phononic modes, we assume a point-like dipole emitter and consider a Jaynes–Cummings Hamiltonian [45–47] under laser illumination

$$\mathbf{H} = \hbar\omega_{\rm ph}\hat{\mathbf{a}}^\dagger\hat{\mathbf{a}} + \tfrac{1}{2}\hbar\omega_{\rm em}\hat{\sigma}_z + \hbar\left[g\hat{\sigma}_+\hat{\mathbf{a}} + f\hat{\mathbf{a}}^\dagger e^{-i\omega t} + \hat{\sigma}_+\Omega e^{-i\omega t} + \text{h.c.}\right], \tag{1}$$

where, for simplicity, we consider a single, hybridized phononic resonance of the whole bowtie antenna rather than two electromagnetically coupled resonances, one for each cone. $\omega_{\rm ph} = 2\pi c/\lambda_{\rm ph}$ and $\omega_{\rm em}$ are the angular frequencies corresponding to the phononic hybridized resonance and the emitter resonance, respectively. c is the speed of light in vacuum, $\hbar$ is the reduced Planck constant and h.c. refers to the Hermitian conjugate. $\hat{\mathbf{a}}$ and $\hat{\mathbf{a}}^\dagger$ are the annihilation and creation operators of the phononic mode, and $\hat{\sigma}_z = |1\rangle\langle 1| - |0\rangle\langle 0|$, $\hat{\sigma}_+ = |1\rangle\langle 0|$, $\hat{\sigma}_- = |0\rangle\langle 1|$ are the Pauli operators of the emitter. Last, g, f and Ω are the coupling constants, g between the emitter and the phononic antenna, and f and Ω between the laser and, respectively, the phononic antenna or the emitter. The laser is treated as a classical plane-wave with incident electric field $E^{\rm i}_{{\rm e},z}e^{-i\omega t}/2 + \text{h.c.}$ polarized along z and evaluated at the position of the emitter $\vec{r}_{\rm e}$. Thus, it is not quantized.

We discuss in the appendix how to obtain the coupling constants. If $1/2(\vec{E}^{\rm s}(\vec{r})e^{-i\omega t} + \text{h.c.})$ and $1/2(\vec{H}^{\rm s}(\vec{r})e^{-i\omega t} + \text{h.c.})$ are the classical scattered electric and magnetic fields at position $\vec{r}$ under plane-wave illumination, obtained from a classical calculation of the isolated antenna and $\omega = \omega_{\rm ph}$, then

$$\begin{aligned}
\Omega &= -\frac{d_z}{\varepsilon_{\rm scr}}\frac{E^{\rm i}_{{\rm e},z}}{2\hbar},\\
g &= -\frac{d_z}{\varepsilon_{\rm scr}}\frac{E^{\rm s}_{{\rm e},z}}{\hbar\,|\,\vec{E}^{\rm s}_{\rm m}\,|}\sqrt{\frac{\hbar\omega_{\rm ph}}{2\varepsilon_0 V_{\rm eff}}},\\
f &= i\frac{\omega_{\rm ph}}{2Q}\sqrt{\frac{\varepsilon_0 V_{\rm eff}}{2\hbar\omega_{\rm ph}}}\,|\,\vec{E}^{\rm s}_{\rm m}\,|\,.
\end{aligned} \tag{2}$$

$E^{\rm s}_{{\rm e},z}/2e^{-i\omega t} + \text{h.c.}$ describes the scattered electric field polarized along z at the position of the emitter, $E^{\rm s}_{{\rm e},z} = \vec{E}^{\rm s}(\vec{r}_e)\cdot 1_z$ with 1_z the corresponding unit vector. $\vec{E}^{\rm s}_{\rm m}/2e^{-i\omega t} + \text{h.c.}$ is the corresponding value describing the maximum of the scattered fields, situated at the gap of the structure. $\vec{E}^{\rm s}(\vec{r})$ and $\vec{H}^{\rm s}(\vec{r})$, and thus $E^{\rm s}_{{\rm e},z}$ and $\vec{E}^{\rm s}_{\rm m}$, do not include the field from the incoming plane-wave. The dipole moment of the emitter d_z always appears scaled by a dimensionless screening factor $\varepsilon_{\rm scr} = (2\varepsilon_0 + \varepsilon_{\rm e})/(3\varepsilon_0)$ to include, for example, the case of a quantum dot emitter made of a semiconductor with a different permittivity $\varepsilon_{\rm e}$ than the surrounding vacuum value ε_0. The scaling by $\varepsilon_{\rm scr}$ corresponds to defining the dipole moment with respect to the fields at

the interior of the emitter [11, 48, 49]. Last, V_{eff} is the effective volume for the phononic mode,

$$V_{\mathrm{eff}} = \frac{\int u_E \,\mathrm{d}V + \int u_H \,\mathrm{d}V}{\varepsilon_0 \mid \vec{E}^{\mathrm{s}}_{\mathrm{m}} \mid^2} \tag{3}$$

with $$u_E = \frac{1}{2}\,\Re\left(\frac{\mathrm{d}\omega'\varepsilon(\vec{r},\omega')}{\mathrm{d}\omega'}\right)\Bigg|_{\omega'=\omega_{\mathrm{ph}}} |\vec{E}^{\mathrm{s}}(r)|^2$$

and $$u_H = \frac{1}{2}\mu\,|\vec{H}^{\mathrm{s}}(r)|^2,$$

where the integrals over the electric (u_E) and magnetic (u_H) energy density [50, 51] extend over the volume inside and outside the bowtie, and ($\frac{\mathrm{d}\omega'\varepsilon(\vec{r},\omega')}{\mathrm{d}\omega'}$) is evaluated at the frequency of the phononic resonance ω_{ph}. $\Re()$ refers to the real part, μ is the vacuum permeability and $\varepsilon(\vec{r},\omega)$ the position-dependent permittivity ($\varepsilon_{\mathrm{SiC}}$ or ε_0). As both the electric and magnetic fields contain a radiative contribution scaling with the inverse of the distance to the antenna, the integrals are infinite. Subtracting the radiative contribution as explained in [52] gives a finite volume; other, more rigorous approaches are also possible [53, 54]. In practice, we find satisfactory results by integrating over a volume of the order of $(\lambda/2)^3$ and using the simple subtraction. For simplicity, the equations assume the coupling constants and the screening factor $\varepsilon_{\mathrm{scr}}$ to be frequency independent. Equation (3) is chosen so that the energy contained by the mode at ω_{ph} equals $\hbar\omega_{\mathrm{ph}}(n+1/2)$, where n is the integer number of excitations in the system. The resulting equation for g can be reduced to the typical expression for dielectric cavities [55] assuming that the integral over the magnetic and electric energy densities are equal. However, these integrals can differ significantly for plasmonic or phononic antennae [56], where the magnetic contribution is often negligible. A more detailed explanation of the derivation of equations (2) and (3) can be found in the appendix.

The Hamiltonian in equation (1) does not include losses or pure dephasing. We use the Lindblad operators $\mathcal{L}_i$ and the density matrix $\hat{\rho}$ to account for these effects [47, 57–59], with the time evolution of the system given by

$$\frac{\mathrm{d}\hat{\rho}}{\mathrm{d}t} = \frac{\mathrm{i}}{\hbar}\,[\hat{\rho}, \mathbf{H}] + \mathcal{L}_1 + \mathcal{L}_2 + \mathcal{L}_3 \tag{4}$$

with $$\mathcal{L}_1 = -\frac{\kappa}{2}(\hat{\mathbf{a}}^\dagger\hat{\mathbf{a}}\hat{\rho} + \hat{\rho}\hat{\mathbf{a}}^\dagger\hat{\mathbf{a}} - 2\hat{\mathbf{a}}\hat{\rho}\hat{\mathbf{a}}^\dagger),$$

$$\mathcal{L}_2 = -\frac{\gamma_{\mathrm{s}}}{2}\left(\hat{\sigma}_+\hat{\sigma}_-\hat{\rho} + \hat{\rho}\hat{\sigma}_+\hat{\sigma}_- - 2\hat{\sigma}_-\hat{\rho}\hat{\sigma}_+\right)$$

and $$\mathcal{L}_3 = -\frac{\gamma_{\mathrm{d}}}{4}\left(\hat{\sigma}_z\hat{\sigma}_z\hat{\rho} + \hat{\rho}\hat{\sigma}_z\hat{\sigma}_z - 2\hat{\sigma}_z\hat{\rho}\hat{\sigma}_z\right) = -\gamma_{\mathrm{d}}\left(\hat{\sigma}_+\hat{\sigma}_-\hat{\rho} + \hat{\rho}\hat{\sigma}_+\hat{\sigma}_- - 2\hat{\sigma}_+\hat{\sigma}_-\hat{\rho}\hat{\sigma}_+\hat{\sigma}_-\right),$$

where γ_{s} and γ_{d} are the spontaneous decay and pure dephasing rate of the emitter, respectively. For an isolated emitter in vacuum, γ_{s} models the decay from the excited to the ground state, and γ_{d} a change in the phase of the quantum state without associated population decay. We assume an emitter with no intrinsic losses, i.e. any decay from the excited to the ground state results in photon emission or phonon excitation. κ is the loss rate of the phononic antenna mode, either from absorption or scattering. It corresponds to the full-width half maximum of the

extinction spectra (as in figure 1(b) but as a function of ω), calculated after performing a simple background subtraction. It relates to the quality factor Q as $Q = \omega_{\rm ph}/\kappa$. The mean emitter and phonon population derive from tracing out $\hat{\rho}$ in the usual manner [46]. The equations assume that the emitter interacts with only one, Lorentzian-like phononic mode, a simplification to be discussed in more detail later.

At this stage, we consider the lowest energy peak of figures 1(b) and (c) at $\lambda_{\rm ph} = 11.695\,\mu$m (106 meV) with $Q \approx 150$ and $\hbar\kappa \approx 690\,\mu$eV. Considering a dipole moment $d_z/\varepsilon_{\rm scr} = 1e$ nm and intensity of the incident plane-wave 1 W m^{-2}, we obtain from equations (2) and (3) $V_{\rm eff} \approx 3.75 \times 10^{-8}\lambda_{\rm ph}^3$, $\hbar g \approx (0.1 - {\rm i}2.3)$ meV, $\hbar\Omega \approx -1.4 \times 10^{-8}$ eV, $\hbar f \approx 8.4{\rm i}\,\mu$eV and $\hbar\gamma_{\rm s} = (8\pi^2 d_z^2)/(3\lambda_{\rm em}^3\varepsilon_0\varepsilon_{\rm scr}^2) \approx 3 \times 10^{-10}$ eV. The condition for strong coupling is $|g| \gtrsim \kappa/4$ (when the phonon is the dominant decay channel) [3, 41]. This condition is verified as long as $d_z/\varepsilon_{\rm scr} \gtrsim 0.075e$ nm. Pure dephasing $\gamma_{\rm d}$ is negligible except when stated otherwise. In practice, steady-state calculations for weak illumination can be correctly performed in the following by assuming low population of the phononic modes.

As a cross-check of the value of g, we can also obtain $|g|$ by equating [41] $1 + 4|g|^2/(\kappa\gamma_{\rm s})$ to the peak enhancement of dissipated power at $\lambda_{\rm ph} = 11.695\,\mu$m in figure 1(c), i.e. to the maximum Purcell factor of the mode under consideration, for weak coupling, no intrinsic losses and no pure dephasing. The difference between the value of g above and the result from the new calculation is less than 1%. The good agreement is achieved despite the limitations discussed in previous work [52] of using the mode volume ($4|g|^2/(\kappa\gamma_{\rm s}) \propto Q/V_{\rm eff}$) to obtain the Purcell factor. We attribute the good agreement to the coupling with a well-defined, isolated Lorentzian-like mode, and to the separate inclusion of both electric and magnetic contributions in the derivation of the obtained equations without assuming that these contributions are equal. For the resonance under analysis, the magnetic energy is negligible. The discrepancy between our two procedures to obtain $|g|$ can become larger for more closely-spaced resonances at larger energies. About 3% differences occur for the mode at $\lambda_{\rm ph} = 10.925\,\mu$m. The agreement at the few per cent level between the two methods to obtain $|g|$ depends to some extent on the exact details of the calculations (for example, how to subtract the background to extract Q).

The considered Jaynes–Cummings Hamiltonian does not capture the Lamb shift [16] due to the interaction and approximates the response by a simple Lorentzian-like mode (we will consider up to three modes later in the paper). An alternative calculation approach to obtain the optical response is to quantize the fields via the Green's function [16, 60]. A classical approach is often also valid to describe strong coupling [61]. However, these classical calculations do not reproduce all the effects predicted by the full quantum treatment as we illustrate below. The Hamiltonian used here is nonetheless useful to understand the underlying physics, and should correctly describe the main effects.

Figures 2(a) and (b) show the steady state population of the emitter and of the phononic mode, for weak illumination of 1 W m^{-2}, $d_z/\varepsilon_{\rm scr} = 1e$ nm and no pure dephasing, as a function of the excitation wavelength $\lambda = 2\pi c/\omega$ and resonant wavelength of the emitter $\lambda_{\rm em} = 2\pi c/\omega_{\rm em}$. A clear anticrossing is observed, with the upper branch changing from phonon-like to emitter-like as the emitter wavelength $\lambda_{\rm em}$ increases, and the lower branch exhibiting the opposite behavior. The simple equation [2, 6, 40] $w_\pm = (\omega_{\rm em} + \omega_{\rm ph})/2 \pm \Re(\sqrt{|\,g\,|^2 + 1/4(\omega_{\rm ph} - \omega_{\rm em} - {\rm i}\kappa/2)^2})$, which ignores emitter losses $\gamma_{\rm s}$ and $\gamma_{\rm d}$, describes well the spectral position of the two branches (green open circles in figure 2(b)). For $\lambda_{\rm em} = \lambda_{\rm ph}$ the energy separation or Rabi splitting between the two branches is large $\approx 2\hbar|g| \approx \hbar\omega_{\rm ph}/23 \approx 4.6$ meV.

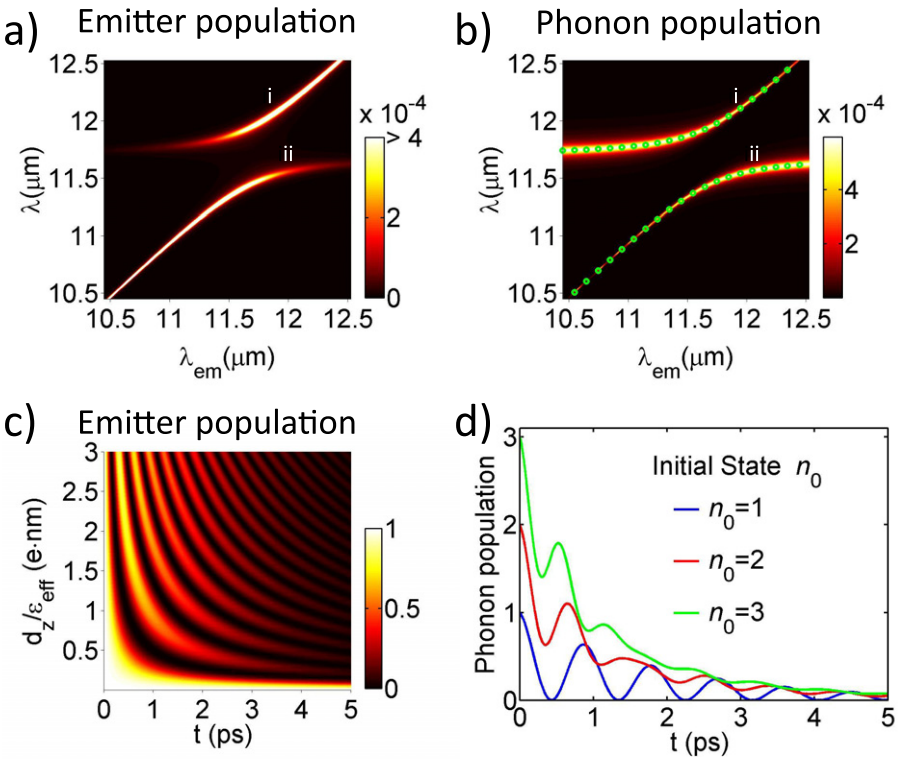

Figure 2. Strong coupling between the emitter and the phononic mode of the SiC bowtie at $\lambda_{\rm ph} = 11.695\,\mu$m. Emitter (a) and phonon (b) population under weak illumination by a plane-wave antenna of intensity $1\,{\rm W\,m^{-2}}$ with electric field parallel to the antenna axis, as a function of the wavelength of the incoming radiation λ and resonant wavelength of the emitter $\lambda_{\rm em}$, for $d_z/\varepsilon_{\rm scr} = 1\,{\rm e\,nm}$. The green open circles in (b) correspond to the simple equation in the text describing the position of the two dispersion branches, labeled (i) and (ii) in (a) and (b). (c), (d) Decay as a function of time of the mean (c) emitter and (d) phonon population, under no excitation. As initial state, in (c) the emitter is populated and no phonon is excited in the SiC antenna, while in (d) the emitter is unpopulated and the SiC antenna phonon population n_0 is 1 (blue line), 2 (red line) or 3 (green line) phonons. Panel (c) is plotted as a function of time t and the screened dipole moment $d_z/\varepsilon_{\rm scr}$, while $d_z/\varepsilon_{\rm scr} = 1e\,{\rm nm}$ for (d). In (c) and (d) $\lambda_{\rm em} = 11.695\,\mu{\rm m}$. Pure dephasing is assumed to be negligible in all cases.

An alternative indication of strong coupling is the presence of vacuum Rabi oscillations in the decay of the system, for no external excitation $f = \Omega = 0$. Figure 2(c) shows the evolution of the emitter population for several values of the screened dipole moment $d_z/\varepsilon_{\rm scr}$ and no pure dephasing, with $\lambda_{\rm em} = 11.695\,\mu{\rm m}$ the initial state corresponding to the emitter in the excited state and an unpopulated phononic mode. For $d_z/\varepsilon_{\rm scr} \gtrsim 1e\,{\rm nm}$ an appreciable number of oscillations are apparent, with a Rabi period $\approx\pi/|g|$. For sufficiently large $d_z/\varepsilon_{\rm scr} \gtrsim 0.2e\,{\rm nm}$, the maximum amplitude of the oscillations decay in a 2 ps ($\approx 2/\kappa$) time scale [40], orders of magnitude faster than the spontaneous emission rate of the emitter ($1/\gamma_{\rm s} \approx 2.2\,\mu{\rm s}$ for $d_z/\varepsilon_{\rm scr} = 1e\,{\rm nm}$). For the weak coupling regime, the increase in the decay rate corresponds to figure 1(c).

A quantum treatment is not necessary to predict the possibility of anticrossing and vacuum Rabi-oscillations, which already appears in more classical treatments of coupled harmonic oscillators [14, 61–65]. In contrast, figure 2(d) reveals an intrinsically quantum effect, the

scaling of the vacuum Rabi frequency [46, 66] with the square root of the integer number of excitations in the system $\sqrt{n}$. In this figure, the initial state corresponds to an unpopulated emitter and to a phonon population n_0 of one, two or three phonons. Figure 2(d) represents the time evolution of the mean phonon population for $d_z/\varepsilon_{\rm scr} = 1e$ nm, no external illumination and no pure dephasing. For $n_0 = 1$, there is one excitation $n = 1$ in the hybrid system until the decay to the ground state occurs, and the obtained time evolution corresponds to a sinusoidal oscillation of exponentially decaying amplitude. The behavior is somewhat more complicated for $n_0 = 2, 3$, where the system can decay into intermediate states at different times before decaying to the ground state. Nonetheless, the initial peaks show a clear oscillatory behavior, with the initial period being, as expected, approximately proportional to $1/\sqrt{n_0}$. This proportionality can be understood from the form of the interaction Hamiltonian for a fixed $n = n_0$ number of excitations (no losses). In this case, the phonon mode population is n_0 or $n_0 - 1$ depending on the state of the emitter and $\hat{\mathbf{a}} = \sqrt{n_0}|n_0 - 1\rangle\langle n_0|$. The emitter–phonon coupling term in the Hamiltonian is then $\hbar g\hat{\sigma}_+\hat{\mathbf{a}} + \text{h.c.} \propto \sqrt{n_0}$, which directly affects the Rabi splitting and the Rabi frequency by the same $\sqrt{n_0}$ factor. It has also been discussed how the population-dependent splitting leads to photon blockade [20], another purely quantum effect.

Up to now, we have considered for simplicity a Hamiltonian that only included the lowest energy phononic mode. The clear anticrossing in figures 2(a) and (b); however, is large enough to be affected by other resonances in the antenna spectral response (figures 1(b) and (c)). We thus include one or two additional modes in a straightforward manner, by incorporating the corresponding terms in the Hamiltonian and Lindblad operators (equations (1) and (4)) to describe the new interactions and losses. To obtain the numerical values of the different coupling strengths and decay rates, we follow the same procedure as for the single mode case as introduced above and detailed in the appendix. We do not include any coupling term between the different phononic modes and neglect any possible mutual interaction via common decay into photons [67].

Figures 3(a) and (b) show the emitter population as in figure 2, but including the effect of the (a) two and (b) three lowest energy phononic modes in figures 1(b) and (c). Besides the resonance at $\lambda_{\rm ph} = 11.695\ \mu$m, the new modes correspond to $\lambda_{\rm ph} = 11.195$ and $10.925\ \mu$m. The number of observed branches (labeled (i)–(iv) in the figures) equals the number of phononic modes considered plus an additional branch due to the emitter transition. The number of anticrossings is one less than the number of branches.

The inclusion of the second phononic mode (figure 3(a)) results in a branch (marked as (ii)) at intermediate energies that is limited by two different anticrossings and, as a consequence, is flatter than the branches found for a single phononic mode (figure 3(a) versus figure 2(a)). Less apparent but possibly more significant, including the second phononic mode ($\lambda_{\rm ph} = 11.195\ \mu$m) modifies the emitter population found for a single mode at excitation wavelengths that, in the absence of the emitter, would only significantly excite the lowest energy mode ($\lambda_{\rm ph} = 11.695\ \mu$m). This behavior points to the possible excitation of a hybrid mode with contributions from the emitter and more than one phononic mode.

We next compare the emitter population for two and three phononic modes (figure 3(a) versus figure 3(b)). The additional mode modifies the emitter population at low energies (corresponding to branches (i) and (ii) in both cases) more weakly, leaving the spectral position of the observed maxima largely unchanged, but it nonetheless influences the exact numerical values. For lower excitation wavelengths ($\lambda \lesssim 11.2\ \mu$m), a second relatively flat branch marked (iii) is observed after including the third phononic mode.

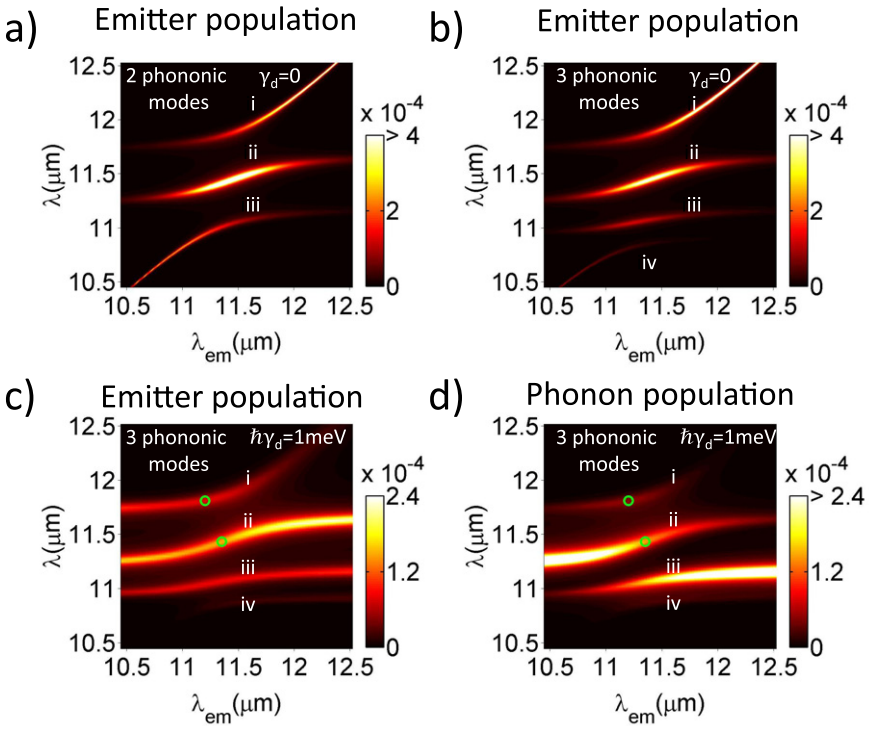

Figure 3. Strong coupling between the emitter and the (a) two or (b)–(d) three lowest energy phononic modes of the SiC bowtie. The three phononic modes correspond to $\lambda_{ph} = 11.695$, 11.195 and 10.925 μm. (a)–(c) Mean emitter population and (d) mean population of the second lowest energy phonon mode under weak illumination by a plane-wave of intensity $1\,\mathrm{W\,m^{-2}}$ and electric field parallel to the antenna axis, as a function of the wavelength of the incoming radiation λ and resonant wavelength of the emitter λ_{em} $d_z/\varepsilon_{scr} = 1e$ nm in all the figures, and the pure dephasing is (a, b) zero or (c, d) $\hbar\gamma_d = 1$ meV. The different resonance branches are labeled (i)–(iv). Green open circles in (c) and (d) correspond to the points ($\lambda_{em} = 11.2\,\mu$m and $\lambda = 11.81\,\mu$m) and ($\lambda_{em} = 11.35\,\mu$m and $\lambda = 11.43\,\mu$m) discussed in the text.

The obtained results should be rather insensitive to pure dephasing, due to the very large coupling constants g between the antenna and emitter. Indeed, a clear anticrossing remains even for rather large pure dephasing $\hbar\gamma_d = 1$ meV, as figures 3(c) and (d) demonstrate for the population of (c) the emitter and (d) the $\lambda_{ph} = 11.195\,\mu$m phononic mode at second lowest energy. Notably, the latter takes a significant value for the lowest energy (i) branch, which is a further indication of the excitation of a complex hybrid mode. To give a more quantitative idea of the nature of this mode, the population of the emitter and of the three considered phononic modes, the latter in order of increasing energy, are $\approx 8.3 \times 10^{-5}$ (upper green circle in figure 3(c)), $\approx 1.84 \times 10^{-4}$, $\approx 5.0 \times 10^{-5}$ (upper green circle in figure 3(d)) and $\approx 4.2 \times 10^{-5}$ for $\lambda_{em} = 11.2\,\mu$m and $\lambda = 11.81\,\mu$m, respectively. The different populations can be more closely balanced in the (ii) branch at slightly larger energies. The corresponding values for this case are $\approx 1.56 \times 10^{-4}$ (lower green circle in figure 3(c)), $\approx 1.46 \times 10^{-4}$, $\approx 1.56 \times 10^{-4}$ (lower green circle in figure 3(d)) and $\approx 7.4 \times 10^{-5}$ for $\lambda_{em} = 11.35\,\mu$m and $\lambda = 11.43\,\mu$m.

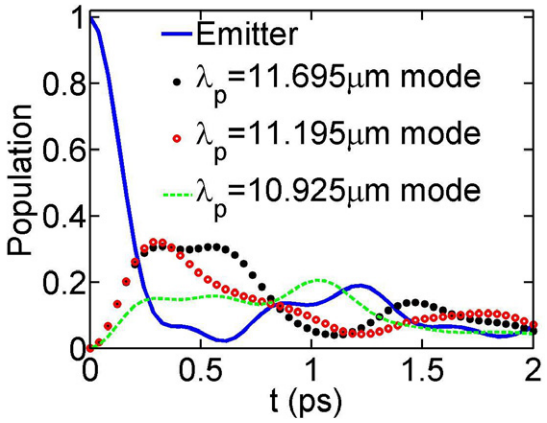

Figure 4. Time evolution of the populations when considering a Hamiltonian including the three lowest energy phononic modes. $\lambda_{em} = 11.35\,\mu$m, $d_z/\varepsilon_{scr} = 1\,e$ nm and $\hbar\gamma_d = 1$ meV. Displayed are the population of the emitter (blue solid line) and the three phononic modes that corresponds to values of λ_{ph} of 11.695, 11.195 and 10.925 μm (black solid circles, red open circles and green dashed line, respectively) under no illumination. The initial state, corresponding to excited emitter and unexcited phononic modes, can be observed from the values at $t = 0$.

This balanced excitation of the different modes contrasts to the behavior in the weak coupling regime, where for a monochromatic laser resonant with one of the lower energy resonant peaks in figure 1(b) the influence of other modes is negligible. Furthermore, in the strong coupling regime, an excitation can oscillate between the emitter and the different phononic modes. Figure 4(a) shows the time evolution of the different populations, for $\lambda_{em} = 11.35\,\mu$m, $\hbar\gamma_d = 1$ meV, no external illumination and considering the three lowest energy phononic modes. Initially, the molecule is in the excited state, and all modes of the SiC antenna are in the ground state. After a first decay from the initial state, clear oscillations are present for all populations and reach maximum values that are of comparable magnitudes, showing energy transfer between all the phononic modes and the emitter.

We have demonstrated, for a Jaynes–Cummings Hamiltonian, the emergence of strong coupling between an emitter and a phononic SiC bowtie antenna. This approach neglects the Lamb shift, but should otherwise adequately describe the coupling. It would also be possible to use this or similar Hamiltonians to study the nonlinear dependence of the response with respect to the excitation intensity [51], the entanglement between different emitters [68], photon correlations [13] or other quantum phenomena. From an experimental perspective, the described SiC bowtie antennae are difficult to fabricate, and we considered dimensions of at least 10 nm to ease the demands. Smaller gaps and sharper bowties should lead to even larger possible coupling strengths, probably at the cost of photon emission becoming weaker with respect to absorption losses. Furthermore, it may prove challenging to exploit single emitters with large dipole moments at the necessary mid-infrared frequencies. Recent work, for example on interband transitions on HgTe [69] quantum dots or intersubband transitions InAs quantum dots [70–72], aim to obtain better emitters at lower energies.

It is possible to demonstrate strong coupling experimentally by measuring vacuum Rabi oscillations or anticrossing. To measure the anticrossing, one method to shift the resonance of the emitter is to change the temperature. A similar alternative would be to shift the wavelength

of the phononic mode by changing the dielectric constant of the surrounding medium [73]. For the studied systems, however, very significant shifts would be necessary. It thus may be easier to reveal the strong coupling by measuring the vacuum Rabi oscillations [74].

Overcoming these obstacles would allow the demonstration of strong coupling of photons with phonon polaritons. It appears possible to obtain modes that are a hybrid of the emitter and more than one phononic mode, a complex hybridization that is also feasible for related plasmonic systems [61]. When other phononic resonances in SiC contribute to the material response $\varepsilon_{\mathrm{SiC}}$ [24, 37] the hybridization may become even more complex. The coupling strengths are very large, and thus the system exhibits short times scales $\approx$1 ps and a significant insensitivity to pure dephasing, which may prove useful, for example, for a source of on-demand single indistinguishable mid-infrared photons emitted at very short time intervals for quantum information applications.

Acknowledgments

RE and JA acknowledge financial support from the project ETORTEK-NanoIker, of the Department of Industry of the Basque Government, from the Spanish National project FIS2010-19609-C02-01E and from the Department of Education of the Basque Government, IT756-13 of consolidated groups. RE acknowledges financial support from the Physics Frontier Center at the Joint Quantum Institute, University of Maryland.

Appendix. Derivation of the coupling constant expressions

In the following we describe in more detail the derivation of the expressions for the coupling strengths for a phononic mode at angular frequency ω_{ph} and a two-level emitter, both placed in vacuum with permittivity ε_0. We aim here for an intuitive understanding instead of a more rigorous derivation [47, 75]. The quantum operators are in the Schrödinger picture, i.e. time independent, with the time t dependence contained in the density matrix.

The emitter, located at $\vec{r}_{\mathrm{e}}$, is small enough for the following assumptions to hold. First, the illuminating and scattered fields vary slowly enough spatially to be treated as constant on the scale of the emitter dimensions. The emitter is thus considered as point-like. For a large emitter, a more complicated procedure may be necessary [76]. Second, if the emitter is made of a dielectric constant different than that of the surrounding vacuum, this dielectric contrast screens the fields but does not affect the resonant mode of the phononic antenna. In a similar manner, we assume that the excitation of the emitter transition does not affect the characteristics of the phononic modes. We thus perform the classical calculations of the phononic antenna under plane-wave illumination in the absence of the emitter to obtain the coupling factors and phononic losses.

We first consider the coupling between an emitter with dipole moment d_z along the z direction and an incident plane-wave at angular frequency ω. The plane-wave is treated classically, polarized along z with electric field at the emitter position $(1/2E^{\mathrm{i}}_{\mathrm{e},z}\mathrm{e}^{-\mathrm{i}\omega t} + 1/2E^{\mathrm{i}^*}_{\mathrm{e},z}\mathrm{e}^{\mathrm{i}\omega t})$, where * indicates the complex conjugate.

We write the resulting interaction Hamiltonian that models the coupling between the emitter and the plane-wave as $\mathbf{H}_{I1} = -(d_z\hat{\sigma}_+ + d_z^*\hat{\sigma}_-)(1/2E^{\mathrm{i}}_{\mathrm{e},z}\mathrm{e}^{-\mathrm{i}\omega t} + 1/2E^{\mathrm{i}^*}_{\mathrm{e},z}\mathrm{e}^{\mathrm{i}\omega t})/(\varepsilon_{\mathrm{scr}})$. The Hamiltonian is time dependent, even if the operators are not, because we have considered

classical fields. $\hat{\sigma}_+$ and $\hat{\sigma}_-$ are the Pauli operators of the emitter. d_z is defined with respect to the fields inside the emitter, so that we divide the fields of the incoming plane-wave by a dimensionless screening factor [11] $\varepsilon_{\rm scr}$. We assume $\varepsilon_{\rm scr}$ is real and frequency independent. In the rotating wave approximation, the fast oscillation terms $\hat{\sigma}_+ e^{i\omega t}$, $\hat{\sigma}_- e^{-i\omega t}$ are ignored. Then, $\mathbf{H}_{I1} = \hbar\hat{\sigma}_+\Omega e^{-i\omega t} + \text{h.c.}$, with $\Omega = -d_z/\varepsilon_{\rm scr}E^{\rm i}_{{\rm e},z}/(2\hbar)$ and h.c. the Hermitian conjugate.

To describe the coupling g between the emitter and the phononic mode, we first relate the electric $\hat{\vec{E}}^{\rm s}(\vec{r})$ and magnetic $\hat{\vec{H}}^{\rm s}(\vec{r})$ field operators of the phononic mode at position $\vec{r}$ to the classical electric $1/2(\vec{E}^{\rm s}(\vec{r})e^{-i\omega_{\rm ph}t} + \vec{E}^{s*}(\vec{r})e^{i\omega_{\rm ph}t})$ and magnetic $1/2\left(\vec{H}^{\rm s}(\vec{r})e^{-i\omega_{\rm ph}t} + \vec{H}^{s*}(\vec{r})e^{i\omega_{\rm ph}t}\right)$ fields associated with the modes. We distinguish operators and classical fields by using '$\hat{}$' for the former. We obtain the fields from classical electromagnetic scattering calculations of the isolated phononic antenna, under the monochromatic plane-wave illumination used to derive Ω, at $\omega = \omega_{\rm ph}$. $\vec{E}^{\rm s}(\vec{r})$ and $\vec{H}^{\rm s}(\vec{r})$ are calculated using the BEM [31], after subtracting the incoming plane-wave from the total fields. We write the corresponding operators

$$\hat{\vec{E}}^{\rm s}(\vec{r}) = \hat{\vec{E}}^{\rm s+}(\vec{r}) + \hat{\vec{E}}^{\rm s-}(\vec{r}) = \sqrt{\frac{\hbar\omega_{\rm ph}}{2\varepsilon_0 V_{\rm eff}}}\left(\frac{\vec{E}^{\rm s}(\vec{r})}{|\vec{E}^{\rm s}_{\rm m}|}\hat{\mathbf{a}} + \frac{\vec{E}^{s*}(\vec{r})}{|\vec{E}^{\rm s}_{\rm m}|}\hat{\mathbf{a}}^\dagger\right), \tag{A.1}$$

$$\hat{\vec{H}}^{\rm s}(\vec{r}) = \hat{\vec{H}}^{\rm s+}(\vec{r}) + \hat{\vec{H}}^{\rm s-}(\vec{r}) = \sqrt{\frac{\hbar\omega_{\rm ph}}{2\varepsilon_0 V_{\rm eff}}}\left(\frac{\vec{H}^{\rm s}(\vec{r})}{|\vec{E}^{\rm s}_{\rm m}|}\hat{\mathbf{a}} + \frac{\vec{H}^{s*}(\vec{r})}{|\vec{E}^{\rm s}_{\rm m}|}\hat{\mathbf{a}}^\dagger\right). \tag{A.2}$$

$|\vec{E}^{\rm s}_{\rm m}|$ corresponds to the maximum value of $|\vec{E}^{\rm s}(\vec{r})|$, which we find at the gap. The superindices +, − indicate the contribution to the $\hat{\vec{E}}^{\rm s}(\vec{r})$, $\hat{\vec{H}}^{\rm s}(\vec{r})$ operators associated with $\hat{\mathbf{a}}$ and $\hat{\mathbf{a}}^\dagger$, annihilation and creation operators, respectively. The prefactor in the right-hand side of equations (A.1) and (A.2) is chosen in analogy of the expression used to quantize light in vacuum or in a dielectric cavity [75]. At this stage, $V_{\rm eff}$ is just a real-valued constant [54] that needs to be found to determine the quantization. From the fields above, the electric W_E and W_H magnetic energy stored by the resonance can be calculated as a volume integral over the corresponding energy density. After neglecting terms $\hat{\mathbf{a}}\hat{\mathbf{a}}$, $\hat{\mathbf{a}}^\dagger\hat{\mathbf{a}}^\dagger$ with a fast time dependence, and considering that the phononic material is dispersive [77],

$$\begin{aligned} W_E &= \frac{1}{2}\int \Re\left(\frac{\mathrm{d}\omega'\varepsilon(\vec{r},\omega')}{\mathrm{d}\omega'}\right)\Big|_{\omega'=\omega_{\rm ph}} \hat{\vec{E}}^{\rm s}\cdot\hat{\vec{E}}^{\rm s}\,\mathrm{d}V \\ &= \frac{\hbar\omega_{\rm ph}}{4\varepsilon_0 V_{\rm eff}}\int \Re\left(\frac{\mathrm{d}\omega'\varepsilon(\vec{r},\omega')}{\mathrm{d}\omega'}\right)\Big|_{\omega'=\omega_{\rm ph}} \left|\frac{\vec{E}^{\rm s}(\vec{r})}{\vec{E}^{\rm s}_{\rm m}}\right|^2 (\hat{\mathbf{a}}\hat{\mathbf{a}}^\dagger + \hat{\mathbf{a}}^\dagger\hat{\mathbf{a}})\,\mathrm{d}V. \end{aligned} \tag{A.3}$$

The corresponding magnetic energy stored is

$$W_H = \frac{1}{2}\int \mu\hat{\vec{H}}^{\rm s}\cdot\hat{\vec{H}}^{\rm s}\mathrm{d}V = \frac{\hbar\omega_{\rm ph}}{4\varepsilon_0 V_{\rm eff}}\int \mu\left|\frac{\vec{H}^{\rm s}(\vec{r})}{\vec{E}^{\rm s}_{\rm m}}\right|^2 (\hat{\mathbf{a}}\hat{\mathbf{a}}^\dagger + \hat{\mathbf{a}}^\dagger\hat{\mathbf{a}})\,\mathrm{d}V. \tag{A.4}$$

$\varepsilon(\vec{r},\omega')$ and μ are the (absolute) permittivity and permeability, respectively. Finally, considering that the total energy $W_E + W_H$ contained in the mode must be $\hbar\omega_{\rm ph}(\hat{\mathbf{a}}^\dagger\hat{\mathbf{a}}+1/2) = \hbar\omega_{\rm ph}/2(\hat{\mathbf{a}}^\dagger\hat{\mathbf{a}}+\hat{\mathbf{a}}\hat{\mathbf{a}}^\dagger)$, we obtain

$$V_{\rm eff} = \frac{\int \frac{1}{2}\,\Re\left(\frac{{\rm d}\omega'\varepsilon(\vec{r},\omega')}{{\rm d}\omega'}\right)\Big|_{\omega'=\omega_{\rm ph}} \mid \vec{E}^{\rm s}(\vec{r}) \mid^2 + \frac{1}{2}\mu \mid \vec{H}^{\rm s}(\vec{r}) \mid^2 \,{\rm d}V}{\varepsilon_0 \mid \vec{E}^{\rm s}_{\rm m} \mid^2}. \tag{A.5}$$

$V_{\rm eff}$ has units of volume, and it simplifies to the usual expression of the effective volume of a dielectric cavity [55] when the magnetic and electric contributions are identical, which is *not* typically the case for phononic or plasmonic structures [51, 56]. Introducing $V_{\rm eff}$ into equation (A.1) and (A.2) from equation (A.5), $\hat{\vec{E}}^{\rm s}(\vec{r})$ and $\hat{\vec{H}}^{\rm s}(\vec{r})$ depend on field ratios.

It is now possible to proceed similarly as for the coupling with the plane-wave. Using the interaction Hamiltonian $\mathbf{H}_{I2} = -(d_z\hat{\sigma}_+ + d_z^*\hat{\sigma}_-)\hat{\vec{E}}^{\rm s}{}_z(\vec{r}_{\rm e})/\varepsilon_{\rm scr}$ and equation (A.1), writing $\vec{E}^{\rm s}_z(\vec{r}_{\rm e}) = E^{\rm s}_{{\rm e},z}$ and neglecting $\hat{\sigma}_+\hat{\mathbf{a}}^\dagger$, $\hat{\sigma}_-\hat{\mathbf{a}}$ terms, one obtains $\mathbf{H}_{I2} = \hbar g\hat{\sigma}_+\hat{\mathbf{a}} + {\rm h.c.}$ with g given by equation (2) in the main text. The z subindex indicates the projection of the corresponding magnitude into this direction.

We describe in the following the derivation of f. We consider the excitation of the isolated phononic system by a plane-wave. In this case, the Hamiltonian is $\mathbf{H} = \hbar\omega_{\rm ph}\hat{\mathbf{a}}^\dagger\hat{\mathbf{a}} + \hbar f\hat{\mathbf{a}}^\dagger{\rm e}^{-{\rm i}\omega t} + \hbar f^*\hat{\mathbf{a}}{\rm e}^{{\rm i}\omega t}$, where the interaction terms are analogous to those in $\mathbf{H}_{I1}$ but for the phonons instead of the single emitter. We solve next the system described by this Hamiltonian. Because we consider illumination by a classical plane-wave, we can obtain f by comparing the results with the classical solution. The density matrix $\hat{\rho}$ satisfies

$$\frac{{\rm d}\hat{\rho}}{{\rm d}t} = \frac{\rm i}{\hbar}\left[\hat{\rho}, \hbar(\omega_{\rm ph}\hat{\mathbf{a}}^\dagger\hat{\mathbf{a}} + f\hat{\mathbf{a}}^\dagger{\rm e}^{-{\rm i}\omega t} + f^*\hat{\mathbf{a}}{\rm e}^{{\rm i}\omega t})\right] - \frac{\kappa}{2}\left(\hat{\mathbf{a}}^\dagger\hat{\mathbf{a}}\hat{\rho} + \hat{\rho}\hat{\mathbf{a}}^\dagger\hat{\mathbf{a}} - 2\hat{\mathbf{a}}\hat{\rho}\hat{\mathbf{a}}^\dagger\right) \tag{A.6}$$

with $\hat{\rho} = \sum_{k,l=0}^{\infty}\rho_{k,l}|k\rangle\langle l|$, $\hat{\mathbf{a}} = \sum_{n=0}^{\infty}\sqrt{n+1}|n\rangle\langle n+1|$ and $\hat{\mathbf{a}}^\dagger = \sum_{n=0}^{\infty}\sqrt{n+1}|n+1\rangle\langle n|$, where the kets and bras refer to the phonon number state. Ignoring nonlinear processes, i.e. $\rho_{k,l} = 0$ for $|k-l| > 1$, we get

$$\begin{aligned}\frac{{\rm d}\rho_{n+1,n}}{{\rm d}t} = \langle n+1|\frac{{\rm d}\hat{\rho}}{{\rm d}t}|n\rangle = {\rm i}\left[-\omega_{\rm ph}\rho_{n+1,n} + f{\rm e}^{-{\rm i}\omega t}\sqrt{n+1}(\rho_{n+1,n+1} - \rho_{n,n})\right] \\ -\frac{\kappa}{2}\left((2n+1)\rho_{n+1,n} - 2\sqrt{(n+2)(n+1)}\rho_{n+2,n+1}\right).\end{aligned} \tag{A.7}$$

Using $\langle\hat{\mathbf{a}}\rangle = {\rm Tr}(\hat{\rho}\hat{\mathbf{a}}) = \sum_{n=0}^{\infty}\sqrt{n+1}\rho_{n+1,n}$ and $\sum_{n=0}^{\infty}\rho_{n,n} = 1$,

$$\frac{{\rm d}\langle\hat{\mathbf{a}}\rangle}{{\rm d}t} = {\rm i}\left[-\omega_{\rm ph}\langle\hat{\mathbf{a}}\rangle - f{\rm e}^{-{\rm i}\omega t}\right] - \frac{\kappa}{2}\langle\hat{\mathbf{a}}\rangle, \tag{A.8}$$

where $\langle\rangle$ indicates the expectation value. Factoring out the fast oscillation $\langle\hat{\mathbf{a}}\rangle = \langle\hat{\mathbf{a}}\rangle'{\rm e}^{-{\rm i}\omega t}$, and taking the steady-state solution ${\rm d}\langle\hat{\mathbf{a}}\rangle'/{\rm d}t = 0$,

$$\langle\hat{\mathbf{a}}\rangle' = \frac{{\rm i}f}{{\rm i}(\omega - \omega_{\rm ph}) - \frac{\kappa}{2}}. \tag{A.9}$$

Using equation (A.9) together with equation (A.1) and evaluating the scattered fields at the position $\vec{r}_m$ of maximum amplitude ($\vec{E}^{\rm s}(\vec{r}_m) = \vec{E}^{\rm s}_{\rm m}$), we obtain for $\omega = \omega_{\rm ph}$

$$\langle \hat{\vec{E}}^{\rm s+}(\vec{r}_m)\rangle = -\sqrt{\frac{\hbar\omega_{\rm ph}}{2\varepsilon_0 V_{\rm eff}}}\frac{\vec{E}^{\rm s}_{\rm m}}{\mid \vec{E}^{\rm s}_{\rm m}\mid}\frac{{\rm i}f}{\frac{\kappa}{2}}{\rm e}^{-{\rm i}\omega_{\rm ph}t}. \tag{A.10}$$

On the other hand, we can simply write the classical scattered fields $\vec{E}^{\rm s}$ at the same position for $\omega = \omega_{\rm ph}$ as

$$\vec{E}^{\rm s}_{\rm m}(\vec{r}_m) = \frac{\vec{E}^{\rm s}_{\rm m}}{2}{\rm e}^{-{\rm i}\omega_{\rm ph}t} + {\rm h.c.} \tag{A.11}$$

$\vec{E}^{\rm s}_{\rm m}$ describes the maximum of the scattered fields at resonance in both equations (A.11) and (A.10). We equate $\vec{E}^{\rm s}_{\rm m}/2\,{\rm e}^{-{\rm i}\omega_{\rm ph}t}$ with $\langle \hat{\vec{E}}^{\rm s+}(\vec{r})\rangle$, and finally obtain

$$f = {\rm i}\frac{\kappa}{2}\sqrt{\frac{2\varepsilon_0 V_{\rm eff}}{\hbar\omega_{\rm ph}}}\frac{\mid \vec{E}^{\rm s}_{\rm m}\mid}{2} = {\rm i}\frac{\omega_{\rm ph}}{2Q}\sqrt{\frac{\varepsilon_0 V_{\rm eff}}{2\hbar\omega_{\rm ph}}}\mid \vec{E}^{\rm s}_{\rm m}\mid, \tag{A.12}$$

where $\kappa = \frac{\omega_{\rm ph}}{Q}$, with Q the quality factor of the phononic mode.

References

[1] Lounis B and Orrit M 2005 Single-photon sources *Rep. Prog. Phys.* **68** 1129–79

[2] Andreani L C, Panzarini G and Gérard J-M 1999 Strong-coupling regime for quantum boxes in pillar microcavities: theory *Phys. Rev.* B **60** 13276–9

[3] Reithmaier J P, Sek G, Löffler A, Hofmann C, Kuhn S, Reitzenstein S, Keldysh L V, Kulakovskii V D, Reinecke T L and Forchel A 2004 Strong coupling in a single quantum dot-semiconductor microcavity system *Nature* **432** 197–200

[4] Yoshie T, Scherer A, Hendrickson J, Khitrova G, Gibbs H M, Rupper G, Ell C, Shchekin O B and Deppe D G 2004 Vacuum rabi splitting with a single quantum dot in a photonic crystal nanocavity *Nature* **432** 200–3

[5] Khitrova G, Gibbs H M, Kira M, Koch S W and Scherer A 2006 Vacuum Rabi splitting in semiconductors *Nature Phys.* **2** 81–90

[6] Hennessy K, Badolato A, Winger M, Gerace D, Atatüre M, Gulde S, Fält S, Hu E L and Imamoglu A 2007 Quantum nature of a strongly coupled single quantum dot–cavity system *Nature* **445** 896–9

[7] Pockrand I, Brillante A and Möbius D 1982 Exciton–surface plasmon coupling: an experimental investigation *J. Chem. Phys.* **77** 6289–95

[8] Bellessa J, Bonnand C, Plenet J C and Mugnier J 2004 Strong coupling between surface plasmons and excitons in an organic semiconductor *Phys. Rev. Lett.* **93** 036404

[9] Sugawara Y, Kelf T A, Baumberg J J, Abdelsalam M E and Bartlett P N 2006 Strong coupling between localized plasmons and organic excitons in metal nanovoids *Phys. Rev. Lett.* **97** 266808

[10] Ambjörnsson T, Mukhopadhyay G, Apell S P and Mikael Käll 2006 Resonant coupling between localized plasmons and anisotropic molecular coatings in ellipsoidal metal nanoparticles *Phys. Rev.* B **73** 085412

[11] Artuso R D and Bryant G W 2008 Optical response of strongly coupled quantum dot–metal nanoparticle systems: double peaked fano structure and bistability *Nano Lett.* **8** 2106–11

[12] Trügler A and Hohenester U 2008 Strong coupling between a metallic nanoparticle and a single molecule *Phys. Rev.* B **77** 115403

[13] Ridolfo A, Di Stefano O, Fina N, Saija R and Savasta S 2010 Quantum plasmonics with quantum dot–metal nanoparticle molecules: influence of the Fano effect on photon statistics *Phys. Rev. Lett.* **105** 263601

[14] Savasta S, Saija R, Ridolfo A, Di Stefano O, Denti P and Borghese F 2010 Nanopolaritons: vacuum Rabi splitting with a single quantum dot in the center of a dimer nanoantenna *ACS Nano* **4** 6369–76
[15] Manjavacas A, García de Abajo F J and Nordlander P 2011 Quantum plexcitonics: strongly interacting plasmons and excitons *Nano Lett.* **11** 2318–23
[16] Van Vlack C, Trøst Kristensen P and Hughes S 2012 Spontaneous emission spectra and quantum light–matter interactions from a strongly coupled quantum dot–metal nanoparticle system *Phys. Rev.* B **85** 075303
[17] Hümmer T, García-Vidal F J, Martín-Moreno L and Zueco D 2013 Weak and strong coupling regimes in plasmonic QED *Phys. Rev.* B **87** 115419
[18] González-Tudela A, Huidobro P A, Martín-Moreno L, Tejedor C and García-Vidal F J 2013 Theory of strong coupling between quantum emitters and propagating surface plasmons *Phys. Rev. Lett.* **110** 126801
[19] Koppens F H L, Chang D E and García de Abajo F J 2011 Graphene plasmonics: a platform for strong light matter interactions *Nano Lett.* **11** 3370–7
[20] Manjavacas A, Nordlander P and García de Abajo F J 2012 Plasmon blockade in nanostructured graphene *ACS Nano* **6** 1724–31
[21] Hillenbrand R, Taubner T and Keilmann F 2002 Phonon-enhanced light–matter interaction at the nanometre scale *Nature* **418** 159–62
[22] Rockstuhl C, Salt M G and Herzig H P 2005 Analysis of the phonon–polariton response of silicon carbide microparticles and nanoparticles by use of the boundary element method *J. Opt. Soc. Am.* B **22** 481–7
[23] Ameen M, Garcia-Etxarri A, Schnell M, Hillenbrand R and Aizpurua J 2010 Infrared phononic nanoantennas: localized surface phonon polaritons in SiC disks *Chin. Sci. Bull.* **55** 2625–8
[24] Caldwell J D *et al* 2013 Low-loss, extreme subdiffraction photon confinement via silicon carbide localized surface phonon polariton resonators *Nano Lett.* **13** 3690–7
[25] Zuloaga J, Prodan E and Nordlander P 2009 Quantum description of the plasmon resonances of a nanoparticle dimer *Nano Lett.* **9** 887–91
[26] Savage K J, Hawkeye M M, Esteban R, Borisov A G, Aizpurua J and Baumberg J J 2012 Revealing the quantum regime in tunnelling plasmonics *Nature* **491** 574–7
[27] Chalopin Y, Dammak H, Hayoun M, Besbes M and Greffet J-J 2012 Size-dependent infrared properties of MgO nanoparticles with evidence of screening effect *Appl. Phys. Lett.* **100** 241904
[28] Mühlschlegel P, Eisler H-J, Martin O J F, Hecht B and Pohl D W 2005 Resonant optical antennas *Science* **308** 1607–9
[29] Farahani J N, Pohl D W, Eisler H-J and Hecht B 2005 Single quantum dot coupled to a scanning optical antenna: a tunable superemitter *Phys. Rev. Lett.* **95** 017402
[30] Neubrech F, Pucci A, Cornelius T W, Karim S, García-Etxarri A and Aizpurua J 2008 Resonant plasmonic and vibrational coupling in a tailored nanoantenna for infrared detection *Phys. Rev. Lett.* **101** 157403
[31] García de Abajo F J and Aizpurua J 1997 Numerical simulation of electron energy loss near inhomogeneous dielectrics *Phys. Rev.* B **56** 15873–84
[32] García de Abajo F J and Howie A 2002 Retarded field calculation of electron energy loss in inhomogeneous dielectrics *Phys. Rev.* B **65** 115418
[33] Palik E 1985 *Handbook of Optical Constants of Solids* (San Diego, CA: Academic)
[34] Spitzer W G, Kleinman D and Walsh D 1959 Infrared properties of hexagonal silicon carbide *Phys. Rev.* **113** 127–32
[35] Le Gall J, Olivier M and Greffet J-J 1997 Experimental and theoretical study of reflection and coherent thermal emission by a SiC grating supporting a surface-phonon polariton *Phys. Rev.* B **55** 10105–14
[36] Nakashima S and Harima H 1997 Raman investigation of SiC polytypes *Phys. Status Solidi* a **162** 39–64
[37] Mutschke H, Andersen A C, Clément D, Henning Th and Peiter G 1999 Infrared properties of SiC particles *Astron. Astrophys.* **345** 187–202
[38] Pitman K M, Hofmeister A M, Corman A B and Speck A K 2008 Optical properties of silicon carbide for astrophysical applications *Astron. Astrophys.* **483** 661–72

[39] Huber A, Ocelic N, Taubner T and Hillenbrand R 2006 Nanoscale resolved infrared probing of crystal structure and of plasmon–phonon coupling *Nano Lett.* **6** 774–8
[40] Auffèves A, Gérard J-M and Poizat J-P 2009 Pure emitter dephasing: a resource for advanced solid-state single-photon sources *Phys. Rev.* A **79** 053838
[41] Auffèves A, Gerace D, Gérard J-M, França Santos M, Andreani L C and Poizat J-P 2010 Controlling the dynamics of a coupled atom–cavity system by pure dephasing *Phys. Rev.* B **81** 245419
[42] Novotny L and Hecht B 2006 *Principles of Nano-Optics* (Cambridge: Cambridge University Press)
[43] Esteban R, Teperik T V and Greffet J J 2010 Optical patch antennas for single photon emission using surface plasmon resonances *Phys. Rev. Lett.* **104** 026802
[44] Chen X-W, Agio M and Sandoghdar V 2012 Metallodielectric hybrid antennas for ultrastrong enhancement of spontaneous emission *Phys. Rev. Lett.* **108** 233001
[45] Savage C M 1990 Quantum optics with one atom in an optical cavity *J. Mod. Opt.* **37** 1711–25
[46] Bruce Shore W and Peter Knight L 1993 The Jaynes–Cummings model *J. Mod. Opt.* **40** 1195–238
[47] Waks E and Sridharan D 2010 Cavity QED treatment of interactions between a metal nanoparticle and a dipole emitter *Phys. Rev.* A **82** 043845
[48] Duan C-K and Reid M F 2006 Dependence of the spontaneous emission rates of emitters on the refractive index of the surrounding media *J. Alloys Compounds* **418** 213–6
[49] Greffet J-J, Hugonin J-P, Besbes M, Lai N D, Treussart F and Roch J-F 2011 Diamond particles as nanoantennas for nitrogen–vacancy color centers arXiv:1107.0502
[50] Derom S, Vincent R, Bouhelier A, Colas des and Francs G 2012 Resonance quality, radiative/ohmic losses and modal volume of mie plasmons *Europhys. Lett.* **98** 47008
[51] Słowik K, Filter R, Straubel J, Rockstuhl C and Lederer F 2013 Strong coupling of optical nanoantennas and atomic systems arXiv:1305.6427
[52] Koenderink A F 2010 On the use of Purcell factors for plasmon antennas *Opt. Lett.* **35** 4208–10
[53] Kristensen P T, Van Vlack C and Hughes S 2012 Generalized effective mode volume for leaky optical cavities *Opt. Lett.* **37** 1649–51
[54] Sauvan C, Hugonin J P, Maksymov I S and Lalanne P 2013 Theory of the spontaneous optical emission of nanosize photonic and plasmon resonators *Phys. Rev. Lett.* **110** 237401
[55] Gérard J-M and Gayral B 1999 Strong Purcell effect for InAs quantum boxes in three-dimensional solid-state microcavities *J. Light. Technol.* **17** 2089–95
[56] Iwase H, Englund D and Vučković J 2010 Analysis of the Purcell effect in photonic and plasmonic crystals with losses *Opt. Express* **18** 16546–60
[57] Lindblad G 1976 On the generators of quantum dynamical semigroups *Commun. Math. Phys.* **48** 119–30
[58] Schirmer S G and Solomon A I 2004 Constraints on relaxation rates for n-level quantum systems *Phys. Rev.* A **70** 022107
[59] Boissonneault M, Gambetta J M and Blais A 2009 Dispersive regime of circuit QED: photon-dependent qubit dephasing and relaxation rates *Phys. Rev.* A **79** 013819
[60] Dung H T, Buhmann S Y, Knöll L, Welsch D-G, Scheel S and Kästel J 2003 Electromagnetic-field quantization and spontaneous decay in left-handed media *Phys. Rev.* A **68** 043816
[61] Pérez-González O, Aizpurua J and Zabala N 2013 Optical transport and sensing in plexcitonic nanocavities *Opt. Express* **21** 15847–58
[62] Pockrand I, Swalen J D, Gordon J G II and Philpott M R 1979 Exciton–surface plasmon interactions *J. Chem. Phys.* **70** 3401–8
[63] Zhu Y, Gauthier D J, Morin S E, Wu Q, Carmichael H J and Mossberg T W 1990 Vacuum Rabi splitting as a feature of linear-dispersion theory: analysis and experimental observations *Phys. Rev. Lett.* **64** 2499–502
[64] Fofang N T, Park T-H, Neumann O, Mirin N A, Nordlander P and Halas N J 2008 Plexcitonic nanoparticles: plasmon–exciton coupling in nanoshell-J-aggregate complexes *Nano Lett.* **8** 3481–7
[65] Novotny L 2010 Strong coupling, energy splitting and level crossings: a classical perspective *Am. J. Phys.* **78** 1199–202

[66] Fink J M, Göppl M, Baur M, Bianchetti R, Leek P J, Blais A and Wallraff A 2008 Climbing the Jaynes–Cummings ladder and observing its nonlinearity in a cavity QED system *Nature* **454** 315–8
[67] Artuso R D and Bryant G W 2013 Quantum dot-quantum dot interactions mediated by a metal nanoparticle: towards a fully quantum model *Phys. Rev.* B **87** 125423
[68] Gonzalez-Tudela A, Martin-Cano D, Moreno E, Martin-Moreno L, Tejedor C and Garcia-Vidal F J 2011 Entanglement of two qubits mediated by one-dimensional plasmonic waveguides *Phys. Rev. Lett.* **106** 020501
[69] Keuleyan S, Lhuillier E and Guyot-Sionnest P 2011 Synthesis of colloidal HgTe quantum dots for narrow mid-IR emission and detection *J. Am. Chem. Soc.* **133** 16422–4
[70] Wasserman D, Ribaudo T, Lyon S A, Lyo S K and Shaner E A 2009 Room temperature midinfrared electroluminescence from InAs quantum dots *Appl. Phys. Lett.* **94** 061101
[71] Passmore B S, Adams D C, Ribaudo T, Wasserman D, Lyon S, Davids P, Chow W W and Shaner E A 2011 Observation of Rabi splitting from surface plasmon coupled conduction state transitions in electrically excited InAs quantum dots *Nano Lett.* **11** 338–42
[72] Liverini V, Nevou L, Castellano F, Bismuto A, Beck M, Gramm F and Faist J 2012 Room-temperature transverse-electric polarized intersubband electroluminescence from InAs/AlInAs quantum dashes *Appl. Phys. Lett.* **101** 261113
[73] Anker J N, Hall W P, Lyandres O, Shah N C, Jing Z and Van Duyne R P 2008 Biosensing with plasmonic nanosensors *Nature Mater.* **7** 442–53
[74] Vasa P, Wang W, Pomraenke R, Lammers M, Maiuri M, Manzoni C, Cerullo G and Lienau C 2013 Real-time observation of ultrafast Rabi oscillations between excitons and plasmons in metal nanostructures with J-aggregates *Nature Photon.* **7** 128–32
[75] Loudon R 2000 *The Quantum Theory of Light* 3rd edn (New York: Oxford University Press)
[76] Andersen M L, Stobbe S, Sørensen A S and Lodahl P 2011 Strongly modified plasmon–matter interaction with mesoscopic quantum emitters *Nature Phys.* **7** 215–8
[77] Jackson J D 1999 *Classical Electrodynamics* 3rd edn (NJ: Wiley)